Hindawi
Structural Control and Health Monitoring
Volume 2023, Article ID 2259575, 16 pages
https://doi.org/10.1155/2023/2259575

Research Article

Bridge Performance Prediction Based on a Novel SHM-Data Assimilation Approach considering Cyclicity

Guang Qu,[1] **Limin Sun**,[2,3] **and Hongwei Huang**[1]

[1]*Department of Bridge Engineering, School of Civil Engineering, Tongji University, 1239 Siping Rd, Shanghai 200092, China*
[2]*State Key Laboratory for Disaster Reduction in Civil Engineering, Tongji University, 1239 Siping Rd, Shanghai, China*
[3]*Shanghai Qi Zhi Institute, Yunjing Road 701, Xuhui, Shanghai 200232, China*

Correspondence should be addressed to Limin Sun; lmsun@tongji.edu.cn

Received 15 December 2022; Revised 18 July 2023; Accepted 13 September 2023; Published 3 October 2023

Academic Editor: Songye Zhu

Modern bridges are monitored by an increasing network of sensors that produce massive data for bridge performance prediction. Reasonably and dynamically predicting with monitored data for the time-variant reliability of the existing bridges has become one of the urgent problems in structural health monitoring (SHM). This study, taking the dynamic measure of structural stress over time as a time series, proposes a data assimilation approach to predicting reliability based on extreme stress data with cyclicity. To this aim, the objectives of this article are to present the following: (a) a Gaussian mixture model-based Bayesian cyclical dynamic linear model (GMM-BCDLM) based on extreme stress data with cyclicity and (b) a dynamic reliability prediction method in the combination of GMM-BCDLM and SHM data via first-order second-moment (FOSM) method. An in-service bridge for providing real-time monitored stress data is applied to illustrate the application and feasibility of the proposed method. Then, the effectiveness and prediction precision of the proposed models are proved to be superior compared to other prediction approaches to extreme stress data with cyclicity.

1. Introduction

In the past two decades, due to the continuous increase in traffic loads and the uncertainties in both mechanical and environmental conditions, health monitoring concepts for bridge systems have become increasingly necessary for the preventive maintenance of new and existing bridges [1–3]. Nowadays, although the monitoring technology has developed for a long time, the performance (e.g., stress, deflection, and reliability) prediction model, based on the data collected by the structure health monitoring (SHM) systems, is still an urgent demand in the current engineering practice, which could assist in the intervention planning (e.g., maintenance, replacement, and rehabilitation) and the cost-optimized aspects on bridges [4–9]. It is not easy to efficiently utilize monitoring data (especially with cyclical trends) for performance prediction. Accordingly, the time-variant SHM data-based dynamic performance prediction, especially involving the monitored cyclical data, is still a grand challenge of the SHM field.

In recent years, diverse forecasting methods have been developed for predicting the dynamic and static structural responses of bridges, which can generally be categorized into model-based methods and data-driven methods [10]. The model-based models often necessitate a prior knowledge of structural features and emphasize the relationship between external excitation and structural responses [11]. For example, Wu et al. [12] proposed an effective method for dynamically predicting long-gauge strains in high-speed railway bridges using fiber Bragg grating (FBG) sensors, based on the finite element approach. This method was validated through numerical simulations, experimental comparisons, and field tests, offering engineers a valuable tool for monitoring the health conditions of high-speed railway bridges. However, the applicability of model-based methods may be limited by the complexity of the mechanical environment and uncertain material properties [13]. Furthermore, due to the complex external environmental factors during operation, the changes in structural parameters may not directly reflect potential structural

damage, therefore, affecting the accuracy and reliability of its real-time application [14].

Data-driven models have gained popularity in recent years, and they establish numerical forecasting models based on field measurement data instead of FE models [15–17]. Based on data mining, a novel time series prediction model with a combination of Kalman filter and autoregressive integrated moving average-generalized autoregressive conditional heteroskedasticity (ARIMA-GARCH) [18] improves the prediction accuracy of bridge structure deformation, which does not meet requirements for predicting nonstationary performance information with cyclical trends. For early warning, a data-driven method based on an improved variational mode decomposition and conditional kernel density estimation to predict the monitoring deformation data avoids exploring the complex internal mechanism of structural behavior evolution [19]. Based on monitoring noncyclical data, bridge structural reliability indices are predicted via a data assimilation method and Bayesian method [20], which is only applicable to nonstationary data without cyclic properties. Besides, another data assimilation method [21] is used to predict long-periodic monitoring information for an in-service bridge. However, the method relies heavily on fixed Fourier function equations, which result in fixed amplitudes for the periods and make it difficult to capture local variations in the real-time monitoring data. As a result, the accuracy of predictions for periodic monitoring data is compromised. Deflection data are also used to provide important information about the structural health condition of bridges with the long short-term memory framework [22], but less attention is paid to the periodicity of the data. In addition, several machine learning methods [23–28] have also been applied to the prediction and early warning based on bridge monitoring data. For example, based on the pavement temperature data of Sutong Bridge, a prediction model based on the long short-term memory neural network was proposed for the prediction and early warning of the bridge state [23]. The problem with these methods is that they need high computational requirements for model training, and if the data used to train a model are biased or unrepresentative, the model will likely exhibit the same biases. These methods mentioned above have a series of limitations and do not provide practical methods for reliability prediction based on cyclical data related to existing monitoring systems. Therefore, finding an algorithm for effectively and dynamically predicting bridge reliability based on the short-periodic monitored information for the daily monitoring of extreme stresses, which could assist in daily bridge maintenance and early warning, is the topic of this study.

Based on the above issues, the following problems need to be solved: (1) the dynamic prediction models based on the cyclical monitored extreme stress data need to be established and (2) the probability recursive processes of dynamic prediction models based on cyclical data need to be achieved.

To predict the time-variant reliability indices of an existing bridge based on the monitoring cyclical extreme stress data, we propose a Gaussian mixture model-based Bayesian cyclical dynamic linear model (GMM-BCDLM) that incorporates initial information and corresponding probability recursion processes. The first step involves establishing a GMM-CDLM model based on initial information. Next, we use the predicted results to update and correct the parameters of the GMM-CDLM model with the Bayesian method during the dynamic prediction of extreme stress. Finally, we use the predicted extreme stress and the first-order second-moment (FOSM) method to dynamically predict the main beam's reliability. The flow plan is shown in Figure 1, and this study is organized as follows: Section 2 proposes the monitored equation and the state equation of CDLM based on extreme stress data with cyclicity. In Section 3, we provide the probabilistic recursion processes of the established CDLM with the Bayesian method based on cyclical data, and then, we provide the recursive processes of the GMM-BCDLM. Section 4 introduces the FOSM method and combines it with the GMM-BCDLM method. Section 5 discusses the application of this method to an existing bridge for performance prediction and compares the effectiveness of the proposed GMM-BCDLM with other methods for monitoring extreme stress data with cyclicity from an actual bridge. Finally, Section 6 concludes this contribution and identifies issues for further examination.

2. The Cyclical Dynamic Linear Model

The cyclical dynamic linear model (CDLM), including a linear cyclical state equation, a monitored equation, and the initial state information, meets the basic assumptions for state-space models [29]. It primarily includes the following assumptions:

(1) A linear approximation of the system is acceptable, and the complete system state can be inferred from the outputs

(2) The process and measurement errors are Gaussian-distributed white noises and are independent and uncorrelated

(3) The state variable $\{\theta_t\}$ is a Markov chain, namely, $\pi(\theta_t \mid \mathbf{D}_{t-1}) = \pi(\theta_t \mid \theta_{0:t-1}, y_{1:t-1}) = \pi(\theta_t \mid \theta_{t-1})$, where $\pi(\bullet)$ is a general probability density function (PDF)

(4) Conditionally on $\{\theta_t\}$, the monitoring data ($\{y_t\}$, $t = 1, 2, 3, \cdots, T$) are independent of each other and y_t depends on θ_t only

2.1. Cyclical-Factor Representation of Periodic Monitoring Data. The linear cyclical state equation shows changes in the system with time and reflects the level of the monitored cyclical extreme stresses and random disturbances. The linear monitoring equation reveals the connection between the monitored extreme stresses and the current state parameters of the system. Moreover, based on the historical monitored extreme stress data, the initial state information can be approximately obtained using the cubical smoothing algorithm with a five-point approximation [30]. In this study, an in-service steel bridge is adopted as the research

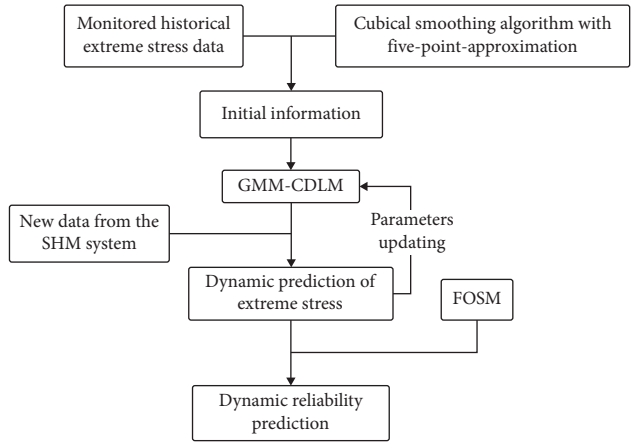

Figure 1: The flow plan of the dynamic reliability prediction method.

object, of which the monitored extreme stress is defined as the monitored maximum stress during each hour.

If the monitored extreme stress data, regarded as a time series, show similarity after p time intervals, such as the peak or trough state at the same time, the series is said to be a cyclical time series with a period of p. There is a general time series set $\mathbf{D}_t$ with period p, which includes the data at and before time t. The state set, also taken as a time series approximately obtained with a cubical smoothing algorithm with five-point approximation through resampling $\mathbf{D}_t$, is denoted by $\mathbf{D}_{\theta_t}$, the ith cyclical differenced data set of which is $\mathbf{D}_{\theta_{t,j}}$. In general, for the nonstationary general time series set $\mathbf{D}_t$ with $(n-1)$-order cyclical trends, the difference can be carried out until the time series after the difference is stationary, and the number $(n-1)$ of difference is the order of cyclical trends. Besides, the augmented Dickey–Fuller (ADF) test method [31] can also help ascertain the stationarity of the data before and after cyclical differences. Let y_t be the monitored extreme stress at time t, the cyclical differences about y_t are

$$\begin{aligned}
\Delta_p^0 y_k &= y_k,\\
\Delta_p^1 y_k &= y_k - y_{k-p},\\
\Delta_p^2 y_k &= \Delta_p^1 y_k - \Delta_p^1 y_{k-p},\\
&\cdots\\
\Delta_p^i y_k &= \Delta_p^{i-1} y_k - \Delta_p^{i-1} y_{k-p},\\
&\cdots\\
\Delta_p^{n-1} y_k &= \Delta_p^{n-2} y_k - \Delta_p^{n-2} y_{k-p},
\end{aligned} \tag{1}$$

where $\Delta_p^i y_k, i = 1, 2, \cdots, n-1; k = 1, 2, \cdots, t$ is the ith order cyclical difference about y_t.

The cyclical factor θ_j, $(j = 0, 1, \cdots, p-1)$ refers to taking p-state values within a cycle. The cyclical vector at time t is the vector that is arranged by cyclical factors in proper order, of which the first element is the cyclical factor at time t, namely,

$$\boldsymbol{\theta}_t = \left(\theta_j, \theta_{j+1}, \cdots, \theta_p, \theta_0, \theta_1, \cdots, \theta_{j-1}\right)^{\mathbf{T}}. \tag{2}$$

In particular, for *arbitrary* natural numbers n and $k = np$, there is

$$\boldsymbol{\theta}_k = \left(\theta_0, \theta_1, \cdots, \theta_{p-1}\right)^{\mathbf{T}}. \tag{3}$$

Let

$$\mathbf{P} = \begin{bmatrix} \mathbf{O} & \mathbf{I} \\ 1 & \mathbf{O} \end{bmatrix} = \begin{bmatrix} 0 & 1 & 0 & \cdots & 0 \\ 0 & 0 & 1 & \ddots & 0 \\ \vdots & \vdots & \ddots & \ddots & 0 \\ 0 & 0 & \cdots & 0 & 1 \\ 1 & 0 & \cdots & 0 & 0 \end{bmatrix}, \tag{4}$$

where $\mathbf{I}$ is a $(p-1)$ order identity matrix and $\mathbf{O}$ means all elements here are zero.

Obviously, $\boldsymbol{\theta}_t = \mathbf{P}\boldsymbol{\theta}_{t-1}$. Also, at time $t-2$, the cyclical-factor vector is

$$\boldsymbol{\theta}_{t-2} = \left(\theta_{j-2}, \theta_{j-1}, \cdots, \theta_p, \cdots, \theta_0, \theta_1, \theta_{j-3}\right)^{\mathbf{T}}. \tag{5}$$

Generally, the cyclical-factor vector at time $t-h$ can be written as

$$\boldsymbol{\theta}_t = P^h \boldsymbol{\theta}_{t-h}. \tag{6}$$

2.2. CDLM Based on Cyclical Extreme Stress Data. Considering the monitored error v_t about y_t conditional on the state (or level), transition error from state to monitoring, and the basic assumptions for state-space models [29], assuming that the monitoring noise and process noise are mutually independent and follow a normal distribution, the CDLM is defined as follows.

Monitored equation:

$$y_t = \mathbf{F}\boldsymbol{\theta}_t + v_t, v_t \sim N[0, V]. \tag{7}$$

State equation:

$$\boldsymbol{\theta}_t = \mathbf{P}\boldsymbol{\theta}_{t-1} + \boldsymbol{\omega}_t, \boldsymbol{\omega}_t \sim \mathrm{N}[0, VW]. \tag{8}$$

Initial information:

$$\left(\boldsymbol{\theta}_{t-1} \mid \mathbf{D}_{t-1}\right) \sim N\left[\mathbf{m}_{t-1}, V\mathbf{C}_{t-1}\right], \tag{9}$$

where y_t is the monitored data at time t; $\boldsymbol{\theta}_t = (\theta_j, \theta_{j+1}, \cdots, \theta_p, \theta_0, \theta_1, \cdots, \theta_{j-1})^{\mathbf{T}}$ is the state cyclical vector at time t; $\mathbf{F} = (1, 0, \cdots, 0)^{\mathbf{T}}$ is a p-dimensional state transfer vector; $N(\cdot)$ represents the Gaussian distribution; v_t and $\boldsymbol{\omega}_{t,i} = [\omega_j, \omega_{j+1}, \cdots, \omega_p, \omega_0, \omega_1, \cdots, \omega_{j-1}]^{\mathbf{T}}$ are, respectively, the monitored white noise and the state cyclical vector of white noises; V is the monitored error variance; $\mathbf{P}$ is a $p \times p$ state transfer matrix, namely, equation (4); W is state error variance estimated by smoothed data; $\mathbf{D}_{t-1}$ is the information set at time $t-1$ and before time $t-1$ [32]; and $\mathbf{C}_{t-1} = \mathrm{diag}(C_{t,0}, \cdots, C_{t,p-1})$ is the $p \times p$ variance matrix of $\boldsymbol{\theta}_{t-1}$.

According to the information provided by the sensor manufacturer, the monitoring error v_t for this type of sensor (pressure transducer) is within 3%. Since it is difficult to precisely determine this error in practical work, for ease of computation, we assume it to be white noise following a normal distribution. Given that the monitoring noise is relatively small, this assumption can approximate the sensor's monitoring noise to a certain extent, providing the model with the uncertainty of monitoring. Furthermore, compared to the monitoring error within 3%, the error introduced by this assumption for monitoring noise can be considered a completely negligible secondary error. And state noise $\boldsymbol{\omega}_{t,i}$ is a stochastic variable introduced in the dynamic model of the system. Its main purpose is to capture uncertainty and random disturbances in our model. State noise is typically assumed to be a zero-mean Gaussian random process with a specific covariance. This means that over the long term, the influence of these noises averages out to zero, but in the short term, they can impact the system state. This aligns with the stress characteristics observed in the monitoring of in-service bridges. Under normal conditions over longer periods (e.g., months or years), the monitored stresses should be stable (with a noise mean of 0). If there are significant fluctuations or trends, it indicates changes in the structural or mechanical environment, requiring further inspection or maintenance.

According to reference [32], W_t can be regarded as a fixed proportion of C_t. This perspective naturally informs our understanding of system variance. Specifically, when an error, $\boldsymbol{\omega}_{t,i} = [\omega_j, \omega_{j+1}, \cdots, \omega_p, \omega_0, \omega_1, \cdots, \omega_{j-1}]^{\mathbf{T}}$, is introduced between observations, this leads to an additive increase in W_t from the initial uncertainty C_t. It is both convenient and intuitive to adopt a constant rate of uncertainty increase, or information decay, for all time points t. Thus, for a given discount factor δ, choose

$$W_t = -C_t + \frac{C_t}{\delta}, \tag{10}$$

where δ is the discount factor, which is usually 0.48–0.98 by the author's experience [33].

2.3. Main Probability Parameters of CDLM. The prior probability parameters of CDLM include V, W_{t-1}, m_{t-1}, and $\mathbf{C}_{t-1}$. The determination approaches are as follows. The relationship between the cyclical factors is only affected by the covariance term of the initial prior and the influence of this initial prior decay with time [33]. Accordingly, for simplicity, suppose $(\boldsymbol{\theta}_0 \mid \mathbf{D}_0) \sim N[\mathbf{m}_0, V\mathbf{C}_0]$, where $\mathbf{m}_0 = m_0\mathbf{I}$ and $\mathbf{C}_0 = C_0\mathbf{I}$ are the initial information, $\mathbf{I}$ is a p-order (p is the period, in this paper $p = 24$) identity matrix, m_0 is the mean value of the initial data, and C_0 is the variance of the initial data, and the initial data are obtained from historical data through the cubical smoothing algorithm with a five-point approximation [30]. Additionally, V is the monitored error variance. $V = 1/n - 1\sum_{i=1}^{n}(y_i - \overline{y})^2$ and n is the number of historical extreme stress data. The reason for using $n-1$ instead of n is that we are calculating the sample variance rather than the population variance.

3. Bayesian Recursive Processes of GMM-CDLM

Based on the established CDLM shown in equations (7)–(9), with the Bayesian method [34, 35], the probability recursion processes and simplified Bayesian recursion processes of CDLM can be reached.

3.1. Probability Recursion Processes of CDLM. To calculate the prior probability, we need to express the joint probability density and then expand it based on conditional probability:

$$p\left(\boldsymbol{\theta}_t, \boldsymbol{\theta}_{t-1} \mid \mathbf{D}_{t-1}\right) = p\left(\boldsymbol{\theta}_t \mid \boldsymbol{\theta}_{t-1}, \mathbf{D}_{t-1}\right) p\left(\boldsymbol{\theta}_{t-1} \mid \mathbf{D}_{t-1}\right). \tag{11}$$

According to the first-order Markov property, we obtain

$$p\left(\boldsymbol{\theta}_t, \boldsymbol{\theta}_{t-1} \mid \mathbf{D}_{t-1}\right) = p\left(\boldsymbol{\theta}_t \mid \boldsymbol{\theta}_{t-1}\right) p\left(\boldsymbol{\theta}_{t-1} \mid \mathbf{D}_{t-1}\right). \tag{12}$$

By further integration to $\boldsymbol{\theta}_t$, we can obtain the marginal probability distribution, i.e., the prior probability distribution:

$$p\left(\boldsymbol{\theta}_t \mid \mathbf{D}_{t-1}\right) = \int p\left(\boldsymbol{\theta}_t \mid \boldsymbol{\theta}_{t-1}\right) p\left(\boldsymbol{\theta}_{t-1} \mid \mathbf{D}_{t-1}\right) \mathrm{d}\boldsymbol{\theta}_{t-1}. \tag{13}$$

Then, to derive the posterior probability distribution, we can expand the joint probability density based on the conditional probability equation (12). And according to the conditional independence, we have

$$p\left(\boldsymbol{\theta}_t, y_t \mid \mathbf{D}_{t-1}\right) = p\left(y_t \mid \boldsymbol{\theta}_t\right) p\left(\boldsymbol{\theta}_t \mid \mathbf{D}_{t-1}\right). \tag{14}$$

The marginal probability density can be obtained by integrating the joint probability density:

$$p\left(y_t \mid \mathbf{D}_{t-1}\right) = \int p\left(y_t \mid \boldsymbol{\theta}_t\right) p\left(\boldsymbol{\theta}_t \mid \mathbf{D}_{t-1}\right) \mathrm{d}\boldsymbol{\theta}_t. \tag{15}$$

Furthermore, the posterior probability distribution is given by

$$p\left(\boldsymbol{\theta}_t \mid \mathbf{D}_t\right) = p\left(\boldsymbol{\theta}_t \mid y_t, \mathbf{D}_{t-1}\right) = \frac{p\left(\boldsymbol{\theta}_t, y_t \mid \mathbf{D}_{t-1}\right)}{p\left(y_t \mid \mathbf{D}_{t-1}\right)} = \frac{p\left(y_t \mid \boldsymbol{\theta}_t\right)p\left(\boldsymbol{\theta}_t \mid \mathbf{D}_{t-1}\right)}{\int p\left(y_t \mid \boldsymbol{\theta}_t\right)p\left(\boldsymbol{\theta}_t \mid \mathbf{D}_{t-1}\right)\mathrm{d}\boldsymbol{\theta}_t}. \tag{16}$$

3.2. Simplified Recursion Processes of CDLM. Referring to [34, 35], Bayesian probabilistic recursion of CDLM means that dynamic recursive processes about CDLM are achieved with the Bayesian method. Also, Bayesian probabilistic recursion is good at inferring and predicting past and future parameters [36].

Based on the aforementioned recursive relationship, under the criterion of minimum mean-square error, the optimal estimate of the value $\boldsymbol{\theta}_t$ is the first moment of the posterior probability density function. The estimate at time t can be written as follows:

$$\widehat{\boldsymbol{\theta}}_t = E\left\{\boldsymbol{\theta}_t \mid \mathbf{D}_t\right\} = \int \boldsymbol{\theta}_t p\left(\boldsymbol{\theta}_t \mid y_1, y_2, \cdots, y_n\right)\mathrm{d}\boldsymbol{\theta}_t. \tag{17}$$

Furthermore, it can be expressed further using equation (8). By applying the method of point estimation [36] and assuming the monitored variance is known, we can simplify the recursive relationship as follows.

Assume time $t = np$, and the current moment is written as $M(0)$.

(1) The prior PDF about the state at time t can be obtained with

$$\left(\boldsymbol{\theta}_t \mid \mathbf{D}_{t-1}\right) \sim N\left(\mathbf{m}_t, R_t\right), \tag{18}$$

where $\mathbf{m}_t = (m_{t,0}, \cdots, m_{t,p-1})^T$, $R_t = C_{t-p,0} + W_t$, and $W_t = -C_{t-p,0} + C_{t-p,0}/\delta$ are calculated and updated with equation (10), and in this study, $\delta = 0.8$.

(2) The one-step forward prediction PDF at time t can be solved with

$$\left(y_t \mid \mathbf{D}_{t-1}\right) \sim N\left(f_t, Q_t\right), \tag{19}$$

where $f_t = \mathbf{F}\mathbf{m}_t = m_{t-p,0}$ is the predicted mean value, $\mathbf{F} = (1, 0, \cdots, 0)^{\mathbf{T}}$ is a p-dimensional state transfer vector, and $Q_t = R_t + V$ is the predicted variance. According to the definition of the highest posterior density (HPD) region [37], the predicted interval of the monitored data m_t with a 95% confidential interval at time t is

$$\left[f_t - 1.96\sqrt{Q_t}, f_t + 1.96\sqrt{Q_t}\right]. \tag{20}$$

(3) With the Bayesian method, the posterior PDF about the state at time t can be calculated with

$$\left(\boldsymbol{\theta}_t \mid \mathbf{D}_t\right) \sim N\left(\mathbf{m}_t, \mathbf{C}_t\right), \tag{21}$$

where $m_{t,0} = m_{t-p,0} + \mathbf{A}_t e_t$, $\mathbf{C}_{t,0} = \mathbf{A}_t$, $\mathbf{A}_t = R_t/(R_t + 1)$, and $e_t = y_t - f_t$. e_t is the one-step forward predicted error and y_t is the monitored data at time t.

Similar equations can be obtained for $M(1)$, $M(2)$, ..., and so on, by simply replacing the subscript 0 with the corresponding subscripts 1, 2, 3, and so forth. The flowchart is shown in Figure 2:

3.3. Gaussian Mixed Model-Based Bayesian Recursive Processes. In practical engineering, the moving loads acting on a bridge and the complexity of the stress environment may cause stress responses to deviate from a normal distribution. In such cases, using only the previously proposed BCDLM may lead to a decrease in prediction accuracy. Considering that Gaussian mixture models (GMMs) can be used to fit and approximate various types of data distributions [38], we have decided to enhance the BCDLM by incorporating a Gaussian mixture model. This improvement allows for a more flexible representation of the input information and improves the modeling accuracy.

For the Gaussian mixed model $M_t(\alpha)$, $A = \{\alpha_1, \alpha_2, \cdots, \alpha_k\}$, $\alpha \in A$, assume the monitored variance V is known. $M_t(\alpha)$ can be written as follows:

$$p\left(\theta_t\right) = \sum_{i=1}^{k} p_t(i) N\left(\theta_t \mid \alpha_i, V_i\right), \tag{22}$$

where $p_t(i)$ represents the weight of the subdistribution of the mixture Gaussian distribution and $\mathrm{N}(\cdot)$ represents the Gaussian distribution.

According to equations (7)–(9) and reference [39], the GMM-CDLM is defined as follows.

Monitored equation:

$$y_t = \mathbf{F}_t(\alpha)\boldsymbol{\theta}_t + \nu_t, \nu_t \sim \mathrm{N}[0, V]. \tag{23}$$

State equation:

$$\boldsymbol{\theta}_t = \mathbf{G}_t(\alpha)\boldsymbol{\theta}_{t-1} + \omega_t, \omega_t \sim N[O, W_t]. \tag{24}$$

Initial information:

$$\left(\boldsymbol{\theta}_{t-1} \mid \boldsymbol{\alpha}, \mathbf{D}_{t-1}\right) \sim N\left[\mathbf{m}_{t-1}(\boldsymbol{\alpha}), V(\boldsymbol{\alpha})\mathbf{C}_{t-1}(\boldsymbol{\alpha})\right], \tag{25}$$

where y_t is the monitored data at time t; $\boldsymbol{\theta}_t = (\theta_j, \theta_{j+1}, \cdots, \theta_p, \theta_0, \theta_1, \cdots, \theta_{j-1})^{\mathbf{T}}$ is the state cyclical vector at time t; $\mathbf{F}_t(\alpha) = (1, 0, \cdots, 0)^{\mathbf{T}}$ is a p-dimensional state transfer vector for the Gaussian mixed model $M_t(\alpha)$; $\mathrm{N}(\cdot)$ represents the Gaussian distribution; ν_t and $\boldsymbol{\omega}_{t,i} = [\omega_j, \omega_{j+1}, \cdots, \omega_p, \omega_0, \omega_1, \cdots, \omega_{j-1}]^{\mathbf{T}}$ are, respectively, the monitored white noise and the state cyclical vector of white noises; V is the monitored error variance; $G_t(\alpha)$ is a $p \times p$ state transfer matrix for the Gaussian mixed model $M_t(\alpha)$, namely, equation (4); W is state error variance estimated by smoothed data; $\mathbf{D}_{t-1}$ is the information set at time $t-1$ and before time $t-1$ [32]; and $\mathrm{C}_{t-1}(\alpha)$ is the $p \times p$ variance matrix of $\boldsymbol{\theta}_{t-1} \mid \alpha$. Also, the variance of state errors can be solved with equation (10).

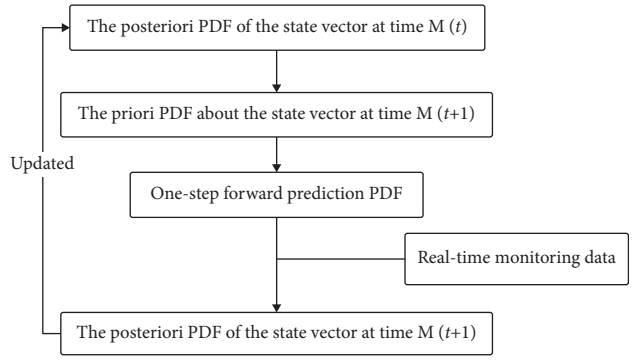

Figure 2: Recursion flowchart of CDLM.

The corresponding recursive processes are as follows:

(1) Assume for each $a_i \in A$, $(\theta_{t-1} \mid \alpha_i, D_{t-1}) \sim N[m_{t-1}(\alpha_i), C_{t-1}(\alpha_i)]$, there are

$$\begin{aligned} \left(\theta_{t-1} \mid \alpha_i, D_{t-1}\right) &\sim N[a_t(\alpha_i), R_t(\alpha_i)], \\ \left(y_t \mid \alpha_i, D_{t-1}\right) &\sim N[f_t(\alpha_i), Q_t(\alpha_i)], \\ \left(\theta_t \mid \alpha_i, D_t\right) &\sim N[m_t(\alpha_i), C_t(\alpha_i)]. \end{aligned} \tag{26}$$

Among them, the mean and variance of each distribution can be recursed and corrected by the model $M(\alpha_i)$ using standard CDLM.

(2) $p(\alpha_i \mid D_{t-1}) = p_{t-1}(i)$ is the posterior probability of selecting the model $M_t(\alpha_i)$ at time $t-1$ and also the prior probability of selecting the model $M_t(\alpha_i)$ at time t.

$$p_t(\alpha_i) = \frac{p\left(y_t \mid \alpha_i, D_{t-1}\right) p_{t-1}(i)}{\sum_{i=1}^{k} p\left(y_t \mid \alpha_i, D_{t-1}\right) p_{t-1}(i)}, \tag{27}$$

where the weight can be calculated with $p(y_t \mid \alpha_i, D_{t-1}) 1/\sqrt{2\pi} e^{-(y_{t-1} - f_{t-1}(\alpha_i))^2 / 2Q_{t-1}(\alpha_i)}$. The initial probability $p_0(i)$ can be given by the EM algorithm [39] and historical data, and the posterior model probability can be continuously corrected.

(3) The prediction PDF at time t can be solved with

$$\left(y_t \mid D_{t-1}\right) \sim \sum_{i=1}^{k} p_t(i) N[f_t(\alpha_i), \theta_t(\alpha_i)]. \tag{28}$$

The predicted mean value at time t is

$$f_t \triangleq \mathrm{E}\left(y_t \mid D_{t-1}\right) = \sum_{i=1}^{k} p_t(i) f_t(\alpha_i). \tag{29}$$

3.4. Components Number Choosing of Gaussian Mixed Model. For a GMM model, if we set the number of components too low, the model may not have enough flexibility to capture the structure of the data, leading to underfitting. On the other hand, if we set the number of Gaussian components too high, the model may become too flexible and lead to overfitting. To strike a balance between underfitting and overfitting, this study employs the Bayesian information criterion (BIC) [40] to determine the optimal number of components in the GMM.

The BIC is defined as follows:

$$\mathrm{BIC} = -2 \cdot \ln(L) + k \ln(n), \tag{30}$$

where L is the likelihood of the data given the model. This represents how well the model fits the data. Higher likelihoods correspond to better fits, so we want to maximize L. k is the number of parameters in the model. This represents the complexity of the model. Models with more parameters are considered more complex. n is the number of data points. $\ln(n)$ is the natural logarithm of the number of data points, which scales the penalty for the number of parameters. Then, by minimizing the BIC, the number of components would be calculated.

3.5. Evaluation of Prediction Precision. In this study, the mean square error (MSE) and normalized root mean square deviation (NRMSD) are adopted to measure the prediction precision. The smaller the MSE and NRMSD, the better the corresponding model. The formulas are as follows:

$$\mathrm{MSE} = \sum_{t=1}^{N} \frac{(f_t - y_t)^2}{N}, \tag{31}$$

$$\mathrm{NRMSD} = \frac{\sqrt{\sum_{t=1}^{N} \left((f_t - y_t)^2 / N \right)}}{(y_{\max} - y_{\min})}, \tag{32}$$

where N is the total number of the predicted data; f_t is the predicted mean value at time t; y_t is the monitored data at time ts; and $y_{\max}$ and $y_{\min}$ are the maximum and minimum monitored data, respectively.

4. Reliability Prediction Based on GMM-BCDLM and FOSM

4.1. FOSM Method. From a safety perspective, within the design service life of civil infrastructure such as bridge structures, the bearing capacity must be greater than the effects caused by various loads acting on it, which the following formula can express as follows:

$$R(X) > S(X), \tag{33}$$

where $R(X)$ represents the structure reactance; $S(X)$ is the load effect (including dead load effect and live load effect) caused by both mechanics and environmental conditions on the structure; and X is various random variables that affect the structure reactance.

Suppose that there are internally independent and mutually independent random variables $R(X)$ and $S(X)$, and the average and standard deviation are μ_A, σ_R, μ_S, and σ_S, respectively.

For the linear limit state functions, the general function of structural performance is

$$Z(X) = R(X) - S(X). \tag{34}$$

According to the central limit theorem, as samples increase, the random variable $Z(X)$ will approach a normal probability distribution. With the FOSM approach [41], the formula of the reliability index can be obtained as

$$\beta = \frac{\mu_R - \mu_S}{\sqrt{\sigma_R^2 - \sigma_S^2}}. \tag{35}$$

4.2. Dynamic Reliability Calculation Formula Based on FOSM and GMM-BCDLM. For this study, the Ningbo Bund bridge, a cable-stayed bridge with a total length of 337 m [42], is chosen as an example. It is important to note that the stress levels at the consolidation part of the tower and beam are significantly higher than in other sections of the structure, requiring special attention. In practical engineering applications, the calculation precision of the FOSM method is deemed sufficient. Under both dead load and live load conditions, the critical section of the main girder experiences static bending failures in both positive and negative bending moments. The sensors of the SHM system for the Ningbo Bund bridge were installed after the bridge was completed, and the monitoring results do not account for the load effect caused by the dead load component. Therefore, when ignoring the influence of geometric parameters, the structural performance function for this steel bridge can be expressed as

$$Z = R - \gamma_M S_M, \tag{36}$$

where R represents the steel yield strength which is 345 MPa for this bridge, and the standard deviation is 27.6 MPa; S_M is the extreme stresses monitored or predicted with time; and $\gamma_M = 1.15$ is a factor assigned to the data provided by sensors [32]. With equations (19) and (34), the predicted dynamic reliability index is

$$\beta = \frac{\mu_R - \gamma_M \mu_M}{\sqrt{\sigma_R^2 + (\gamma_M \sigma_M)^2}}, \tag{37}$$

where (μ_R, σ_R) is, respectively, the mean and standard deviation of R; (μ_M, σ_M) is, respectively, the mean and standard deviation of S_M; and γ_M is a factor assigned to the data provided by sensors. Especially, when equation (37) is used to calculate the reliability indices based on monitored extreme stress data, σ_M is the standard deviation of the monitoring information.

5. Application to an Existing Bridge

5.1. Bridge Introduction. The Ningbo Bund Bridge, situated in downtown Ningbo, China, is depicted in Figure 3. It is a single-pylon four-plane special-type cable-stayed bridge with a main span of 225 m, primarily composed of a separated steel-box girder [42]. The bridge is predominantly made of steel, with an allowable stress of 345 MPa, and its support conditions are specified in reference [42]. The health monitoring system is connected to an off-site data acquisition station and utilizes a fiber-optic network provided by a telecommunications company to transmit data to the Urban Bridge Monitoring and Management Center in Ningbo City for storage and management. Subsequently, the management center conducts data preprocessing to enhance data quality.

The stress measurement points of this bridge are arranged with two cross sections, respectively, the main beam section at the consolidation part of the tower and beam (measurement points STR1-16) and the root section at the front tower column of the cable tower (measurement points STR17-24). The sensors used in this study are pressure transducers, which convert pressure signals into electrical signals for transmission and processing. These pressure sensors are equipped with temperature compensation functionality and are installed and calibrated by the supplier during bridge construction. This allows for effective calibration of the sensor readings and reduces the impact of temperature changes on the measurement accuracy of the sensors.

The section at the consolidation part of the tower and beam is critical in controlling the safety-based structural performance and is monitored by the stress sensors for the longitudinal stress information. The pressure transmitters are mounted on the crossbeam reinforcement rib inside the steel-box girder using bolt fasteners. These pressure transmitters are equipped with temperature compensation functionality and have been precalibrated by the manufacturer during installation. This calibration capability enables the sensors to correct monitoring readings and minimize the impact of temperature fluctuations on measurement accuracy. The layout of measurement points in this section is shown in Figure 4. It can be seen that these sensors, STR1-16, are located on the same steel beam and are connected in series. As the failure of any monitoring section leads to the collapse of the entire girder, the failure modes of the monitoring sections of the bridge girder are considered a series structure. This steel box girder represents an n-dimensional series system with n correlated failure modes. Due to their almost identical

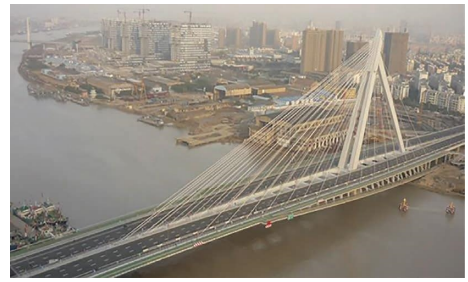

Figure 3: A view of Ningbo Bund bridge.

mechanical environment, they have a strong correlation. For the convenience of calculation, it is assumed that they are fully correlated, and the failure probability p_f of the main beam system can be simplified as follows:

$$\begin{aligned} &P\left(Z_{1,t} \le 0, Z_{2,t} \le 0, \cdots, Z_{n,t} \le 0\right) \\ &= \max\left(P\left(Z_{1,t} \le 0\right), P\left(Z_{2,t} \le 0\right), \cdots, P\left(Z_{n,t} \le 0\right)\right) \\ &= \max p_{f_i}, \quad i = 1, 2, \cdots, n, \end{aligned} \tag{38}$$

where $Z_{i,t}$ ($i = 1, 2, \ldots, n$) represents the performance function calculated with equation (36) and $P(Z_{i,t} \le 0) = p_{f_i}$ is the failure probability of sections at the location $i = 1, 2, \cdots, n$.

Among these monitoring points, point STR1 stands out as the most critical point and is, therefore, chosen as the focal point of our research. The average stress levels monitored at this point are notably higher compared to other points. Based on equation (38), the failure probability at monitoring point STR1 is found to be the highest, making its reliability indices indicative of the overall reliability of the main beam. The hourly monitored extreme stress data collected by the sensor STR1, shown in Figure 5, are utilized to establish the CDLM for Bayesian dynamically predicting the extreme hourly stress at point STR1.

Bridge monitoring information generally exhibits dynamic characteristics, randomness, and periodicity due to the effects of periodic temperature load and peak traffic flow. Based on the real-time monitoring information of the STR1 measurement point of this cable-stayed bridge, the CDLM is established. In May 2020, the point STR1 was dynamically monitored with a 1 Hz sampling frequency of sampling rate, and the extreme hourly stress was utilized to establish the CDLM for Bayesian dynamically predicting the extreme hourly stress at the dangerous point STR1 of the main beam section. While a higher sampling frequency can provide more accurate measurements of instantaneous stress changes, in this study, we focus on the extreme stress values per hour, which can be considered as long-term statistical data relative to 1 Hz sampling data. In this case, collecting a sufficient number of data samples can compensate to some extent for the lower sampling frequency's limitations in capturing instantaneous responses and provide an accurate estimation of extreme stress values per hour.

5.2. Predictive Results of GMM-BCDLM. Our objective is to develop a model that accurately captures the structural response characteristics and exhibits a certain level of generalization to ensure efficiency in real-time applications. By utilizing only 240 hours of data for model validation, we can further demonstrate the efficient utilization of response information by the model and the high computational efficiency of the model itself.

To dynamically predict the reliability of the main beam section based on monitored extreme stresses, we divided the detailed procedures into three steps: (a) hourly monitored extreme stresses of the former 240 h for sensor STR1 are used to establish GMM-CDLM; (b) the mean value of extreme hourly stresses from the 241st hour to 360th hour is predicted with equations (22)–(29); and (c) with equations (35)–(38) and the prediction results, the prediction reliability indices of the main beam are computed.

With (1), the first-order cyclical difference about y_t can be obtained (see Figure 6), which is stationary after the augmented Dickey–Fuller (ADF) test [31].

Through the cubical smoothing algorithm, hourly extreme stress data of the former 240 h are approximately resampled into initial state data (see Figure 7). Then, the established cyclical dynamic linear model, with equations (2)–(9) and (24)–(26), can be obtained as follows.

The monitored equation is similar to (18), where $\mathbf{F}_t(\alpha) = (1, 0, \cdots, 0)^{\mathrm{T}}$ is a 24-dimensional state transfer vector.

The state equation is similar to (24), where $\mathbf{G}_t(\alpha)$ is a 24×24 state transfer matrix obtained with equation (4), $W_t = C_{t-p+1,0}(\delta^{-1} - 1)$, and according to the experience of the author, $\delta = 0.8$.

The initial state information can be obtained using a cubical smoothing algorithm with five-point approximation [30] applied to the previous 240 h extreme stress data, and initial parameters are then determined with equations (22) and (25) and Section 2.3. Finally, the density estimation $p_0(i)$ is obtained via the expectation-maximization algorithm [39] and initial state data.

Then, with equations (7)–(29) and updating, the predicted hourly extreme stress mean value about the hourly monitoring extreme stresses is computed and shown in Figure 8, which indicates that the predicted results fit the changing rules of monitored extreme stress data well and remain within the 95% confidence interval.

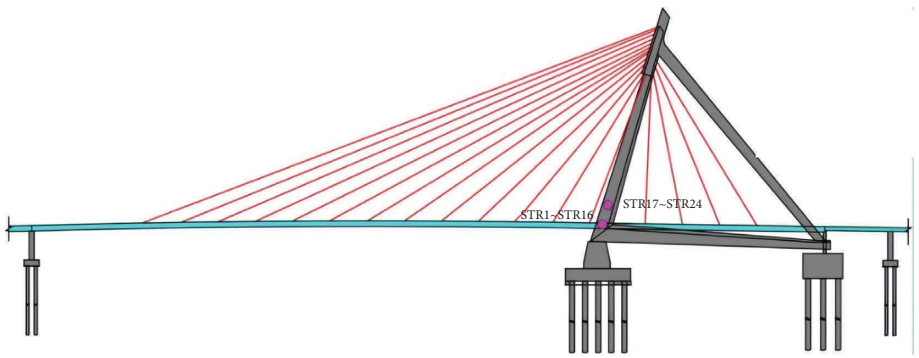

Figure 4: Monitored sections for Ningbo Bund bridge.

Figure 5: The sensor layout at the critical section.

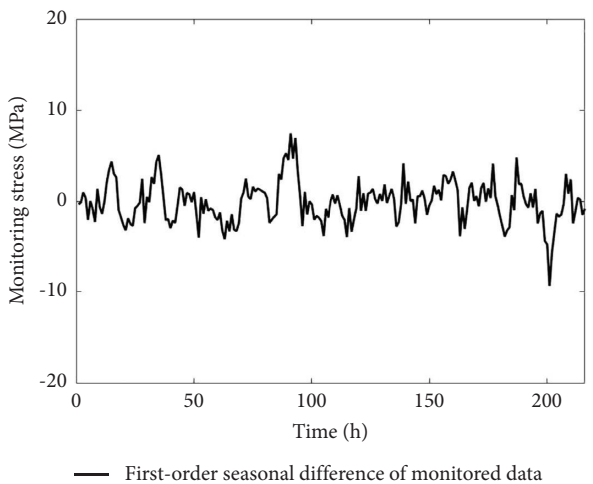

Figure 6: First-order cyclical difference of monitored extreme stress data.

When establishing a predictive model based on normal historical data, the expected prediction will also reflect the structural behavior trends of a bridge's normal operation. By using prediction intervals, the range of potential trends can be further determined. If the monitoring data deviate from this expected trend, particularly beyond a certain confidence interval (typically 95% or 99.7%), it indicates the possibility of sensor or even structural anomalies, necessitating further inspection.

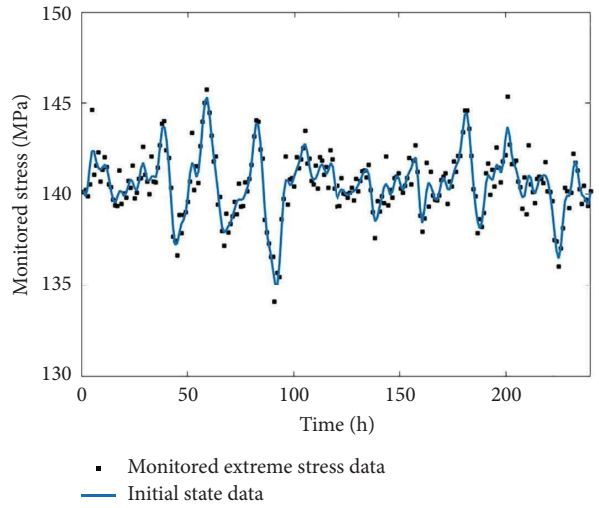

Figure 7: Monitored extreme stresses and initial state data of STR1.

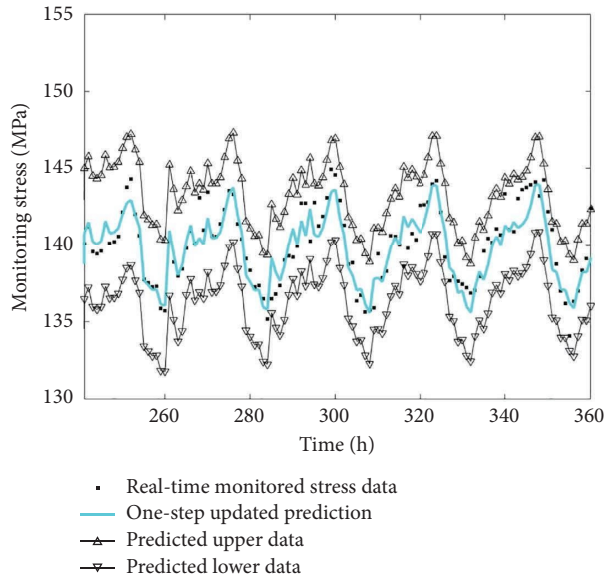

Figure 8: Monitored data, predicted results, and range of hourly extreme stress of STR1.

5.3. Analysis of Prediction Results. In Figure 9, we show different prediction results of four existing common approaches for a fair comparison, i.e., GMM-BCDLM, Bayesian Fourier dynamic linear model (BFDLM) [32], seasonal autoregressive and moving average model (SARMA) [43], and long short-term memory (LSTM) [22] to forecast extreme stress data with cyclicity. It indicated the superiority and advantages of the proposed method for monitored data with cyclicity.

To further demonstrate the effectiveness of the proposed model in this paper, two additional sensors, STR2 and STR10, were selected as research objects. The GMM-CDLM model was established to model and predict their behavior and compared with other commonly used methods. The predicted results are shown in Figures 10 and 11.

With equations (31)–(32), the computed MSE and NRMSD results for GMM-BCDLM, BFDLM, SARMA, and LSTM are shown in Tables 1 and 2, respectively. Among these, the proposed GMM-BCDLM model yields the smallest MSE and NRMSD, thereby indicating superior predictive performance. This further underscores the enhanced accuracy of our proposed model in predicting cyclical bridge structural monitoring information.

It can be observed that in Figure 10, during the period from 280 hours to 300 hours, two measured data points lie far away from the predicted curve. We have included these points in Figure 12 and added a 95% confidence prediction interval. It is important to understand that a 95% confidence prediction interval means that there is a 95% probability of the actual values falling within this interval. Therefore, it is

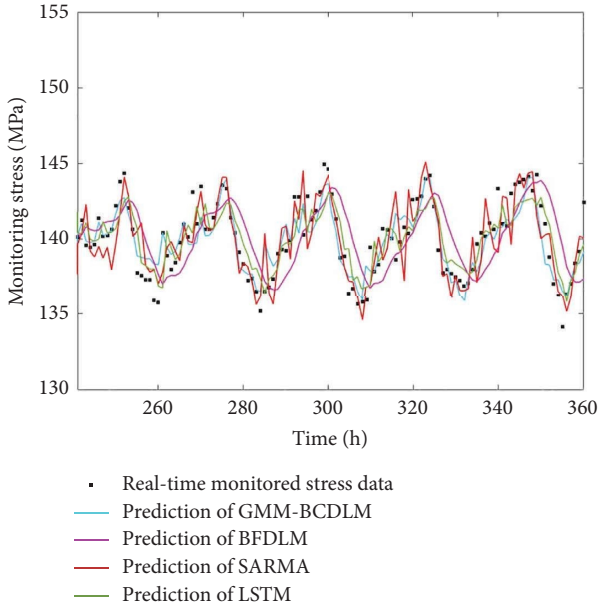

Figure 9: Comparison between BFDLM, SARMA, LSTM, and GMM-BCDLM.

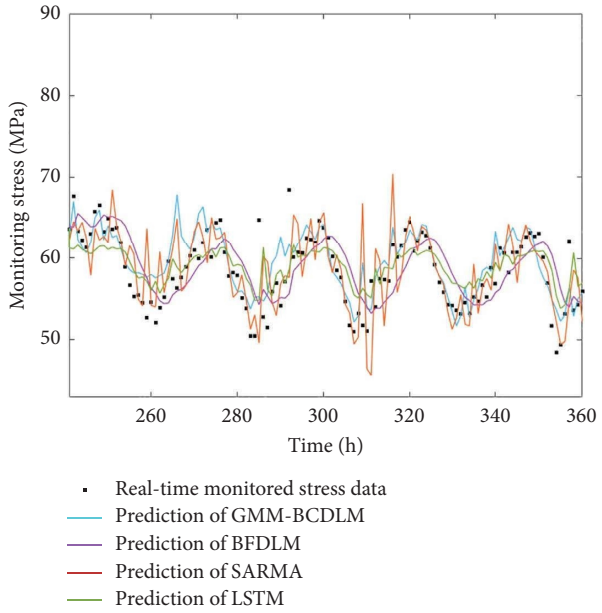

Figure 10: Comparison between the four methods (sensor STR2).

still consistent with our expected outcome, considering that only a few data points out of 120 deviate from the predicted interval.

The choice of a 95% confidence interval is primarily for analytical convenience. In practical engineering applications, higher confidence levels are often employed to determine warning thresholds. A commonly used choice is a 99.7% confidence interval, corresponding to the 3-sigma criterion. By adjusting the confidence level, it is possible to determine reasonable warning thresholds based on engineering considerations.

Here are the prediction interval results with a 99.7% confidence level (Figure 13). It can be observed that as the confidence level increases, the possibility of false alarms is

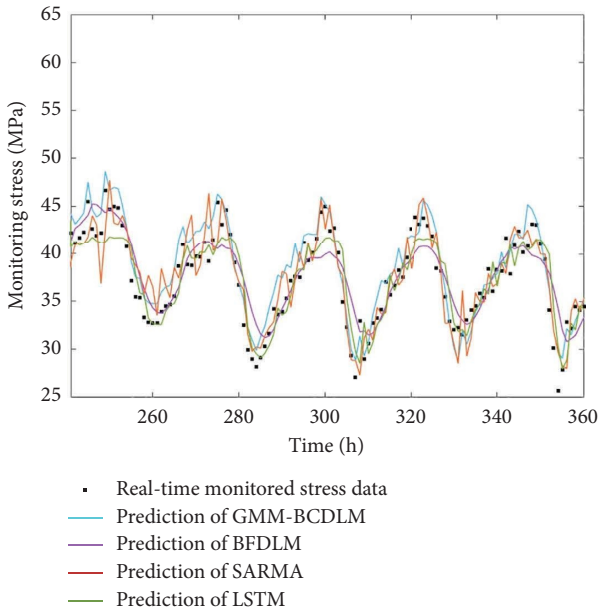

Figure 11: Comparison between the four methods (sensor STR10).

Table 1: MSEs of the different models.

	GMM-BCDLM	BFDLM	SARMA	LSTM
Sensor STR1	1.993	5.0441	2.6809	2.0748
Sensor STR2	8.8690	13.7649	16.7401	10.6454
Sensor STR10	4.0601	6.4653	6.0648	4.8587

Table 2: NRMSDs of the different models.

	GMM-BCDLM	BFDLM	SARMA	LSTM
Sensor STR1	0.1304	0.4658	0.2476	0.1916
Sensor STR2	0.1849	0.2303	0.2540	0.2025
Sensor STR10	0.0964	0.1216	0.1178	0.1054

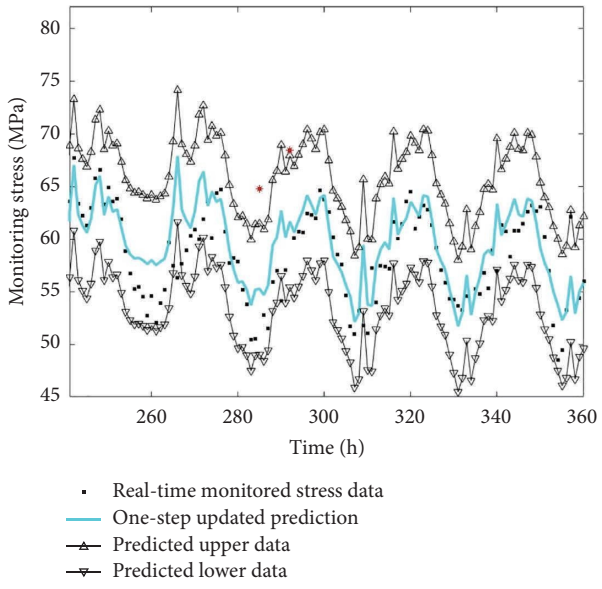

Figure 12: Prediction results with 95% confidence prediction interval (sensor STR2).

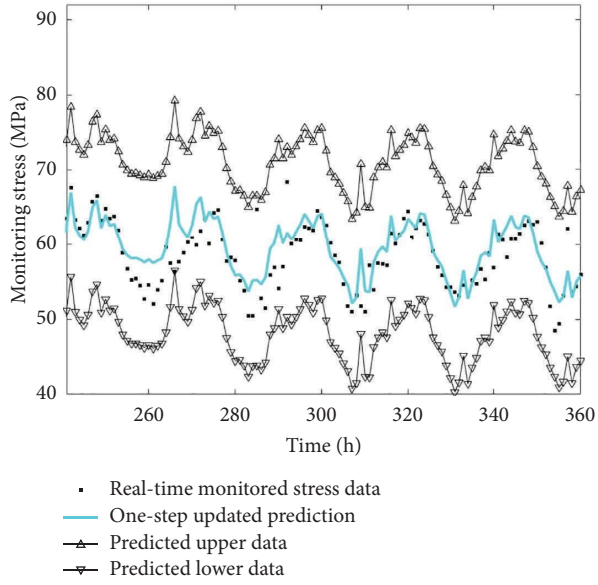

Figure 13: Prediction results with 99.7% confidence prediction interval (sensor STR2).

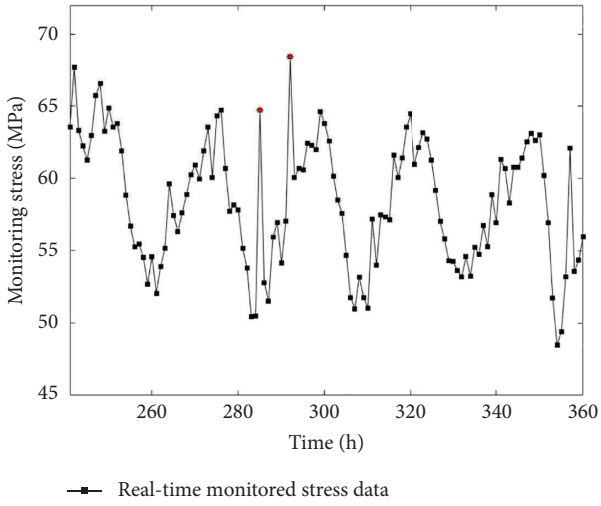

Figure 14: Original monitored data (sensor STR2).

significantly reduced. We further focus our attention on the raw data (Figure 14), where it can be seen that the stress monitoring values exhibit a substantial increase in an area where they should have been at a lower level within the cycle. This could reasonably be attributed to the passing of an overloaded vehicle or a sensor anomaly. However, considering the acceptable range relative to the warning threshold (taking the 99.7% confidence prediction interval as an example), it falls within an acceptable range. If the monitoring values were to further increase and even exceed the warning threshold, such as the range within the 99.7% confidence interval, it could be classified as an exceptional case requiring further inspection or repair at the STR2 section of the main beam.

5.4. Reliability Prediction. With equations (19) and (38), the predicted and monitored reliability indices are, respectively, calculated. Furthermore, according to (38), the reliability indices of monitoring point STR1 can represent the

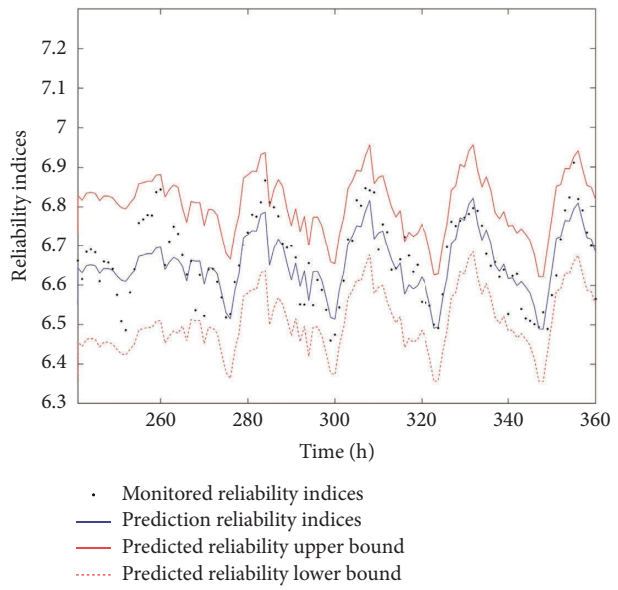

Figure 15: Monitored reliability indices and GMM-BCDLM-based predicted reliability indices.

reliability of the entire main beam. Comparing the predicted reliability indices with the statistical monitoring values at a 95% confidence level [37], the predicted results, as shown in Figure 15, are in good agreement with the monitored reliability indices. The predicted reliability indices are all above 5.2, indicating the safety of the main beam.

6. Conclusions

This article proposes a new prediction approach, a Gaussian mixture model-based Bayesian cyclical dynamic linear prediction method, to dynamically predict the performance of steel bridges based on extreme stresses with cyclicity. GMM-CDLM is first built in the analysis processes, and the corresponding probability recursion method is given in detail with the Bayesian approach. The monitoring data of the steel bridge are provided to illustrate the effectiveness of the proposed method. The prediction results illustrate that the proposed method can make dynamic predictions based on monitored data with cyclicity and has excellent prediction precision. Monitored data with cyclicity refer to the type of data collected from the monitoring sensors that exhibit periodic or cyclic patterns over time. In the context of our study, it refers to the monitored data from the bridge's sensors, which demonstrate repetitive variations over a specific time interval, associated with recurring factors of daily cycles. Usually, the simplest way to identify cyclicity is by plotting the data and visually identifying any apparent patterns, as seen in the monitored data of this study. If there is a need to satisfy this condition mathematically, statistical analysis (autocorrelation analysis to quantitatively assess the presence of periodic patterns) or spectral analysis (like Fourier analysis) methods are commonly employed.

However, some limitations should be noted. Although our method has been validated through critical components of actual bridges, the correlation between sensors has not been studied quantitatively. Future work should include follow-up studies to consider the dependency between sensors.

Data Availability

All data included in this study are available from the corresponding author upon request.

Conflicts of Interest

The authors declare that they have no conflicts of interest.

Acknowledgments

This work was supported by the National Natural Science Foundation of China (Project no. 51878482).

References

[1] M. M. Futai, T. N. Bittencourt, H. Carvalho, and D. M. Ribeiro, "Challenges in the application of digital transformation to inspection and maintenance of bridges," *Structure and Infrastructure Engineering*, vol. 18, no. 10-11, pp. 1581–1600, 2022.

[2] D. M. Frangopol, A. Strauss, and S. Kim, "Bridge reliability assessment based on monitoring," *Journal of Bridge Engineering*, vol. 13, no. 3, pp. 258–270, 2008.

[3] P. Miao, "Prediction-based maintenance of existing bridges using neural network and sensitivity analysis," *Advances in Civil Engineering*, vol. 2021, Article ID 4598337, 17 pages, 2021.

[4] P. Mazurek, "A comprehensive review of steel wire rope degradation mechanisms and recent damage detection methods," *Sustainability*, vol. 15, no. 6, p. 5441, 2023.

[5] J. Dodson, A. Downey, S. Laflamme et al., "High-rate structural health monitoring and prognostics: an overview," in *Proceedings of the Data Science in Engineering, Volume 9: Proceedings of the 39th IMAC, A Conference and Exposition on*

Structural Dynamics 2021, pp. 213–217, Springer International Publishing, Berlin, Germany, April 2022.

[6] Y. M. Zhang, H. Wang, Y. Bai, J. X. Mao, and Y. C. Xu, "Bayesian dynamic regression for reconstructing missing data in structural health monitoring," *Structural Health Monitoring*, vol. 21, no. 5, pp. 2097–2115, 2022.

[7] Y. Tian, Y. Xu, D. Zhang, and H. Li, "Relationship modeling between vehicle-induced girder vertical deflection and cable tension by BiLSTM using field monitoring data of a cable-stayed bridge," *Structural Control and Health Monitoring*, vol. 28, no. 2, Article ID e2667, 2021.

[8] X. Wang, C. Miao, and X. Wang, "Prediction analysis of deflection in the construction of composite box-girder bridge with corrugated steel webs based on MEC-BP neural networks," *Structures*, vol. 32, pp. 691–700, 2021.

[9] Z. Chen, T. Guo, G. Zhou, X. Liu, Y. Fu, and H. Liu, "Time-dependent reliability assessment of long-span PSC box-girder bridge considering vehicle-induced cyclic creep," *Journal of Bridge Engineering*, vol. 28, no. 4, Article ID 04023011, 2023.

[10] Q. A. Wang, C. Zhang, Z. G. Ma, and Y. Q. Ni, "Modelling and forecasting of SHM strain measurement for a large-scale suspension bridge during typhoon events using variational heteroscedastic Gaussian process," *Engineering Structures*, vol. 251, Article ID 113554, 2022.

[11] F. I. Sakiyama, G. S. Veríssimo, F. Lehmann, and H. Garrecht, "Quantifying the extent of local damage of a 60-year-old prestressed concrete bridge: a hybrid SHM approach," *Structural Health Monitoring*, vol. 22, no. 1, pp. 496–517, 2023.

[12] B. Wu, Z. Lin, Y. Liang, Z. Zhou, and H. Lu, "An effective prediction method for bridge long-gauge strain under moving trainloads with experimental verification," *Mechanical Systems and Signal Processing*, vol. 186, Article ID 109855, 2023.

[13] G. Jiang, Q. Liang, H. Wang et al., "Study on evaluation theory of bridge damage state and methodology on early warning of danger," *Advances in Materials Science and Engineering*, vol. 2022, Article ID 6636959, 11 pages, 2022.

[14] H. Zhao, C. Tan, E. J. Obrien, B. Zhang, N. Uddin, and H. Guo, "Developing digital twins to characterize bridge behavior using measurements taken under random traffic," *Journal of Bridge Engineering*, vol. 27, no. 1, Article ID 04021101, 2022.

[15] H. Yao, S. Zhao, Z. Gao et al., "Data-driven analysis on the subbase strain prediction: a deep data augmentation-based study," *Transportation Geotechnics*, vol. 40, Article ID 100957, 2023.

[16] A. Ghaderi and R. Dargazany, "A data-driven model to predict constitutive and failure behavior of elastomers considering the strain rate, temperature, and filler ratio," *Journal of Applied Mechanics*, vol. 90, no. 5, Article ID 051010, 2023.

[17] N. E. Silionis and K. N. Anyfantis, "Data-driven probabilistic quantification and assessment of the prediction error model in damage detection applications," *Probabilistic Engineering Mechanics*, vol. 71, Article ID 103412, 2023.

[18] J. Xin, J. Zhou, S. X. Yang, X. Li, and Y. Wang, "Bridge structure deformation prediction based on GNSS data using Kalman-ARIMA-GARCH model," *Sensors*, vol. 18, no. 1, p. 298, 2018.

[19] J. Xin, Y. Jiang, J. Zhou, L. Peng, S. Liu, and Q. Tang, "Bridge deformation prediction based on SHM data using improved VMD and conditional KDE," *Engineering Structures*, vol. 261, Article ID 114285, 2022.

[20] Y. Liu and X. Fan, "Bayesian prediction of bridge extreme stresses based on DLTM and monitoring coupled data," *Structural Health Monitoring*, vol. 19, no. 2, pp. 454–462, 2020.

[21] Y. Liu and X. Fan, "A data assimilation method about Bayesian Fourier dynamic linear prediction of periodic extreme stresses for steel bridges," *Mechanical Systems and Signal Processing*, vol. 128, pp. 82–92, 2019.

[22] C. Wang, F. Ansari, B. Wu, S. Li, M. Morgese, and J. Zhou, "LSTM approach for condition assessment of suspension bridges based on time-series deflection and temperature data," *Advances in Structural Engineering*, vol. 25, no. 16, pp. 3450–3463, 2022.

[23] A. Guo, A. Jiang, J. Lin, and X. Li, "Data mining algorithms for bridge health monitoring: kohonen clustering and LSTM prediction approaches," *The Journal of Supercomputing*, vol. 76, no. 2, pp. 932–947, 2020.

[24] J. Shu, D. Zhao, X. Zheng, Y. Li, and Y. Zhang, "Bridge temperature prediction model based on long-short term memory neural network," *Journal of Physics: Conference Series*, vol. 1966, 2021.

[25] Y. Zhang and Y. Lei, "Data anomaly detection of bridge structures using convolutional neural network based on structural vibration signals," *Symmetry*, vol. 13, no. 7, p. 1186, 2021.

[26] R. Zhang, L. Meng, Z. Mao, and H. Sun, "Spatiotemporal deep learning for bridge response forecasting," *Journal of Structural Engineering*, vol. 147, no. 6, Article ID 04021070, 2021.

[27] J. Peng, S. Zhang, D. Peng, and K. Liang, "Application of machine learning method in bridge health monitoring," in *Proceedings of the2017 Second International Conference on Reliability Systems Engineering (ICRSE)*, pp. 1–7, IEEE, Beijing, China, July 2017.

[28] S. Xiao, S. Qiao, H. Chen et al., "Data prediction model based on LSTM neural network in bridge health monitoring system IOP Conference Series: earth and Environmental Science," *IOP Conference Series: Earth and Environmental Science*, vol. 668, no. 1, Article ID 012068, February 2021.

[29] M. West and J. Harrison, *Bayesian Forecasting and Dynamic Models*, Springer series, New York, NY, USA, second edition, 1997.

[30] S. S. Siddiqi and N. Ahmad, "A new five-point approximating subdivision scheme," *International Journal of Computer Mathematics*, vol. 85, no. 1, pp. 65–72, 2008.

[31] R. H. Shumway and D. S. Stoffer, *Time Series Analysis and its Applications with R Examples*, Springer series, New York, NY, USA, 2010.

[32] G. Qu, *Research on Dynamic Prediction Methods of Bridge Extreme Stresses Based on Monitoring Data Assimilation*, Doctoral dissertation, School of Civil Engineering and Mechanics, Lanzhou University, Lanzhou, China, 2019.

[33] F. Khan, S. Ali, A. Saeed, R. Kumar, and A. W. Khan, "Forecasting daily new infections, deaths and recovery cases due to COVID-19 in Pakistan by using Bayesian Dynamic Linear Models," *PLoS One*, vol. 16, no. 6, Article ID e0253367, 2021.

[34] M. West, "Bayesian dynamic modelling. Bayesian Inference and Markov chain Monte Carlo," *Honour of Adrian FM Smith*, vol. 145, p. 166, 2013.

[35] X. Zhang, F. Liu, C. Zhang, and Y. Ge, *Bayesian Dynamic Model and its Prediction*, Shandong Science and Technology Press, Shandong, China, 1992.

[36] G. Best and R. Fitch, "Bayesian intention inference for trajectory prediction with an unknown goal destination," in *Proceedings of the 2015 IEEE/RSJ International Conference on Intelligent Robots and Systems (IROS)*, pp. 5817–5823, IEEE, Hamburg, Germany, September 2015.

[37] L. Joseph, D. B. Wolfson, and R. D. Berger, "Sample size calculations for binomial proportions via highest posterior density intervals," *The Statistician*, vol. 44, no. 2, pp. 143–154, 1995.

[38] Y. Xie, L. Peng, Z. Chen, B. Yang, H. Zhang, and H. Zhang, "Generative learning for imbalanced data using the Gaussian mixed model," *Applied Soft Computing*, vol. 79, pp. 439–451, 2019.

[39] M. R. Gupta and Y. Chen, "Theory and use of the EM algorithm," *Foundations and Trends® in Signal Processing*, vol. 4, no. 3, pp. 223–296, 2010.

[40] S. Kucuksari and N. Erdogan, "Modeling and data analysis of electric vehicle fleet charging," in *Proceedings of the 2022 IEEE Transportation Electrification Conference & Expo (ITEC)*, pp. 1139–1143, IEEE, Anaheim, CA, USA, June 2022.

[41] A. H.-S. Ang and W. H. Tang, *Probability Concepts in Engineering Planning and Design*, Wiley, New York, NY, USA, 1984.

[42] Z. Yanli, C. Liangchun, and L. Dechuan, "Key Construction Techniques for Structure of Irregular cable-stayed Bridge in Ningbo Bund Bridge," *Technology of Highway & Transport*, vol. 2012, no. 2, pp. 75–78, 2012.

[43] M. Hupez, J. F. Toubeau, Z. De Grève, and F. Vallée, "SARMA time series for microscopic electrical load modeling," in *Advances in Time Series Analysis and Forecasting: Selected Contributions from ITISE 2016 3*, pp. 133–145, Springer International Publishing, Berlin, Germany, 2017.